

Coupling mechanisms in double sandbar systems. Part 2: Impact on alongshore variability of inner- bar rip channels

Bruno Castelle^{1,2*}, B. G. Ruessink³, Philippe Bonneton^{1,2}, Vincent Marieu^{1,2}, Nicolas Bruneau^{1,2} and Timothy D. Price³

¹ CNRS, UMR EPOC 5805, Talence, F-33405, France

² Université de Bordeaux, UMR EPOC 5805, Talence, F-33405, France

³ Institute for Marine and Atmospheric Research, Department of Physical Geography, Utrecht University, The Netherlands

Received 22 April 2009; Revised 14 September 2009; Accepted 15 October 2009

*Correspondence to: Bruno Castelle, CNRS, UMR EPOC 5805, Talence, F-33405, France. E-mail: b.castelle@epoc.u-bordeaux1.fr

ESPL

Earth Surface Processes and Landforms

ABSTRACT: Double sandbar systems are common morphological features along sandy, wave-dominated, micro- to meso-tidal coastlines. In the companion paper, we demonstrated how various alongshore inner-bar rip-channel patterns can develop through morphological coupling to an alongshore-variable outer bar. The simulated coupling patterns are, however, scarcely observed in the field. Instead, inner-bar rip channels more often possess remarkably smaller and more variable alongshore length scales, suggesting that coupling mechanisms do not play a substantial role in the overall double-sandbar dynamics. Here we use a numerical model to show that the relative importance of self-organization and morphological coupling changes in favour of the latter with an increase in waterdepth variability along the outer-bar crest. Furthermore, we find that the typical alongshore variability in inner-bar rip-channel scale is indicative of a mixture of self-organization and morphological coupling rather than self-organization alone. Morphological coupling may thus be more important to understanding and predicting the evolution of inner-bar rip channels than previously envisaged. Copyright © 2010 John Wiley and Sons, Ltd.

KEYWORDS: self-organization; forcing templates; morphological coupling; rip channel variability; double sandbar system

1 Introduction

Surf zone sandbars protect beaches from wave attack by dissipating wave energy offshore through depth-induced wave breaking. Their morphology guides and constrains nearshore wave-induced currents such as rip current circulations (MacMahan *et al.*, 2005), resulting in erosion features known as mega-cusps (Short and Hesp, 1982; Thornton *et al.*, 2007). Therefore, understanding and predicting rip channel dynamics is relevant for shoreline evolution, localized beach and dune erosion during storms and safety implications. Sometimes, the alongshore variability of the sandbar geometry is low (Greenwood and Davidson-Arnott, 1979; Short, 1991). This alongshore-uniform shape is often observed during a storm event when the three-dimensional (3D) bar is rapidly reshaped into a shore-parallel linear bar (Wright and Short, 1984; Lippmann and Holman, 1990; Van Enckevort *et al.*, 2004). Most of the time, surfzone sandbars exhibit striking 3D patterns which can be described in the convenient morphodynamic framework of Wright and Short (1984). The rhythmic or quasi-rhythmic 3D patterns can be viewed as an alongshore sequence of horns (shoals) and bays (cross-shore troughs) where horns extend landward and bays seaward (Van Enckevort *et al.*, 2004) with a wavelength on the order of several times the surf zone width. The resulting patterns are

the so-called crescentic sandbars and rip channels. Recently, in the framework of the recent paradigm shift from template forcing theory to self-organization mechanisms (Coco and Murray, 2007), both linear stability models (Deigaard *et al.*, 1999; Falqués *et al.*, 2000; Damgaard *et al.*, 2002; Calvete *et al.*, 2005) and nonlinear morphodynamic models (Damgaard *et al.*, 2002; Reniers *et al.*, 2004; Castelle *et al.*, 2006; Klein and Schuttelaars, 2006; Drønen and Deigaard, 2007; Garnier *et al.*, 2008; Smit *et al.*, 2008) have established that these 3D surfzone sandbars can be formed through self-organization mechanisms alone, and do not require a template in the hydrodynamics, as was previously proposed with the edge wave theory (Bowen and Inman, 1971; Holman and Bowen, 1982).

Double sandbar systems are common morphological features along sandy, wave-dominated, micro- to meso-tidal coastlines (Lippmann *et al.*, 1993; Barousseau *et al.*, 1994; Ruessink *et al.*, 2003; Van Enckevort *et al.*, 2004; Castelle *et al.*, 2007). In the cross-shore direction, the interactions between bars in multiple-barred settings have been recently touched upon. The observations of Ruessink and Terwindt (2000) and numerical modelling of Aarninkhof *et al.* (1998) and Masselink (2004) indicated that the morphodynamic feedback, driven for example by the position and geometry of one sandbar with respect to a second, might be a critical parameter

governing the behaviour of the whole system. Surprisingly, both the inner- and outer-bar rip channels and crescentic planshapes are nowadays believed to be free instabilities of the nearshore system arising through self-organization mechanisms alone, with the interaction of a given bar with respect to another barely touched upon until very recently. In double sandbar systems, the inner bar has been observed to possess remarkably smaller and more variable alongshore scales than the outer bar (e.g. Bowman and Goldsmith, 1983; Van Enckevort *et al.*, 2004), suggesting the absence of interaction and a self-organization at the scale of the individual bar (Houser and Greenwood, 2005). In the companion paper (Castelle *et al.*, 2010, noted as Part 1 below), we showed that the dynamics of inner-bar rip channels are potentially more complicated than they would be if they were governed by self-organization mechanisms alone. The authors showed that alongshore variability in outer-bar depth, and the relative importance of wave breaking versus wave focusing by refraction across the outer bar is crucial to the inner-bar rip channel development. A new mechanism that blurs the distinction between self-organization and template forcing theories (Coco and Murray, 2007) was proposed to explain the formation of previously observed coupling patterns in the field (Van Enckevort and Wijnberg, 1999; Castelle *et al.*, 2007). The simulated coupling patterns, emerging from morphological coupling mechanisms, were essentially similar to the existing observations.

Clear coupling patterns in double sandbar systems, such as those presented in Van Enckevort and Wijnberg, 1999; Castelle *et al.*, 2007; Quartel, 2009 and Part 1), are however rarely observed in the field (Homma and Sonu, 1962; Goldsmith *et al.*, 1982; Bowman and Goldsmith, 1983). More often, inner-bar rip channels possess remarkably smaller and more variable alongshore scales than the outer bar (Barousseau *et al.*, 1994; Van Enckevort *et al.*, 2004; Lafon *et al.*, 2004, 2005). Figure 1 shows a typical double sandbar system geometry with an outer bar exhibiting crescentic patterns at a narrow range of wavelength, which contrasts with highly alongshore-variable inner-bar rip channels. This widely observed characteristic would suggest that morphological coupling does not play a substantial role in the overall double-sandbar dynamics. Ruessink *et al.* (2007) recently examined an eight-week dataset of daily time-exposure video images, starting from an alongshore-uniform double sandbar configuration following a storm event. Using a wavelet analysis, the authors showed that the initial inner bar and outer bar 3D pattern developments were spatially non-coupled. However, over time, the inner-bar morphology appeared to couple with that of the outer bar, with the inner bar patterns developing in response to the increasingly three-dimensional, onshore

propagating outer bar. This suggests that the outer-bar geometry is a critical parameter governing the morphological evolution of the composite double sandbar system.

This is Part 2 of a two-part paper on morphological coupling in the nearshore. In Part 1, we introduced and explored morphological coupling. Here, we examine the relative importance of morphological coupling and self-organization to the generation of inner-bar rip channels. We use the same numerical model as in Part 1, but now add small initial perturbations to the seabed to allow for the growth of inner-bar rip channels through self-organization mechanisms. Our model results and a wavelet analysis (next section) demonstrate that, as suggested by the observations of Ruessink *et al.* (2007), the variability in mean water depth along the outer bar controls the relative importance of self-organization mechanisms versus morphological coupling mechanisms and, hence, is crucial to the evolution of inner-bar rip channels (Results section).

2 Method

2.1 Model set-up, initial bathymetries and grid

The modelling strategy used in this study is essentially similar to that detailed in Part 1: a nonlinear morphodynamic model that couples a spectral wave model (Booij *et al.*, 1999), a time- and depth-averaged flow model (Castelle *et al.*, 2006), an energetic-type sediment transport model (Bailard, 1981), and the bed level continuity equation to compute bed level changes.

We ran the model for three different double sandbar geometries on a computational grid with an alongshore length of 4200 m, 20×20 m grid cells, and periodic lateral boundary conditions. In each geometry, we implemented an alongshore-uniform inner bar, 100 m from the mean-sea-level shoreline and with its crest in 1 m water depth. The three different outer-bar geometries were an alongshore-uniform outer bar, a well-developed outer crescentic bar, and a weakly developed outer crescentic bar. For the alongshore-uniform geometry, the outer bar was located 250 m from the mean-sea-level shoreline with its crest in 3 m water depth. In the two non-uniform geometries, crescentic patterns with a wavelength of 600 m were superimposed on the alongshore-uniform configuration as an alongshore sequence of horns and bays alternating shoreward and seaward of the outer bar crest. In both geometries, the cross-shore distance between a horn and a bay amounted to 60 m. For the weakly developed geometry, the vertical amplitude of the bay/horn sequence was 0.2 m, which we increased to 1.5 m for the well-developed geometry. The bars are superimposed on a 1:50 planar sloping depth profile, with its offshore extent in 10.5 m water depth. In contrast with the simulations in Part 1, we superimposed random perturbations with a magnitude of a few centimetres in the seabed to investigate the relative importance of self-organization at the scale of the individual bar versus coupling mechanisms. We note that the alongshore-uniform geometry is essentially similar to previous modelling experiments (Klein and Schuttelaars, 2006; Drønen and Deigaard, 2007; Smit *et al.*, 2008), who all examined the initial growth of crescentic patterns in double sandbars but did not investigate the potential importance of morphological coupling to inner-bar patterns in case of pre-existing outer-bar crescentic patterns.

We ran all the simulations for offshore significant wave heights H_{s0} of 0.8 m and 1 m, a peak period of 8 s, shore-normal incidence and time-invariant mean water level (no tide). These offshore wave conditions were motivated by the

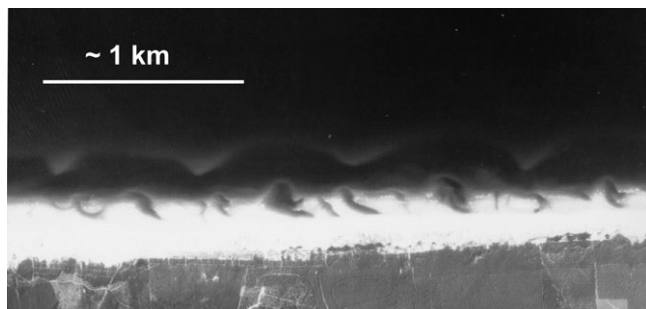


Figure 1. Aerial photograph of a double sandbar system on the French Aquitanian Coast displaying alongshore regularly spaced outer-bar crescentic patterns which contrast with highly alongshore-variable inner-bar rip channels.

simulations in Part 1, which showed that coupling patterns arise from horizontal circulation patterns driven by alongshore variations in wave set-up enforced by wave refraction and depth-induced breaking over the outer bar. The relative importance of wave focusing by refraction versus wave breaking across the outer bar was proven to control the inner-bar patterns morphologically forced by the outer bar. The authors additionally showed that, when wave breaking overwhelms wave focusing by refraction across the outer bar, 180° out-of-phase coupling emerges regardless of the outer-bar wavelength. When wave focusing by refraction overwhelms wave breaking, coupling at half of the outer-bar wavelength (in phase) is observed for larger (smaller) outer-bar wavelength and larger (smaller) vertical amplitude of the horn and bay sequence. According to Part 1, for the given outer-bar wavelength $\lambda = 600$ m and when investigating coupling mechanism alone (i.e. without initial superimposed perturbations of the seabed), waves with $H_s = 0.8$ m (1 m) are likely to favour coupling at half of the outer-bar wavelength (180° out-of-phase coupling). In this paper we ran, as mentioned in section 3, an additional simulation with an outer-bar crest in 2 m water depth and $H_s = 1.6$ m for the alongshore-uniform case to investigate the change of the double sandbar system behaviour from non-coupled to coupled, as observed in Ruessink *et al.* (2007). As we will see below, both $H_s = 0.8$ and 1.0 m are too low to modify the initial outer-bar morphology. The larger H_s in the non-coupled to coupled run was invoked to cause the initially alongshore-uniform outer bar to develop 3D patterns in time, which may potentially cause the inner-bar rip channels to change from self-organized into morphologically coupled features. As detailed in Part 1, there is no bed diffusion or bedslope transport in our model to damp the seabed instabilities. Continuing the simulations over a long duration would make the bed slope locally too large and the sandbar morphology unrealistic. Accordingly, when investigating the relative importance of self-organization mechanisms versus morphological coupling, we analysed the double sandbar morphology when the mean alongshore height variation of the alongshore depth line Z_{inner} (Figure 2), representative of the inner-bar morphology, reached about 0.5 m. This means that here we do not consider any steady state of the double sandbar system. Given that we ran the model for different wave conditions and initial alongshore non-uniformities (outer-bar geometry), the run durations given below ranged from 4 to 12 days.

2.2 Wavelet Analysis

To examine inner-bar rip channels and their potential coupling to the outer-bar crescents in more detail, we used a wavelet analysis. We applied the continuous wavelet transforms $W_n^z(s)$ defined as the convolution of a discrete sequence z_n ($n = 0, \dots, N - 1$) with a scaled and normalized mother wavelet function ψ_0 :

$$W_n^z(s) = \left(\frac{dz}{s}\right)^{1/2} \sum_{n'=0}^{N-1} z_{n'} \psi_0^* \left\{ \frac{(n' - n) dz}{s} \right\}, \quad (1)$$

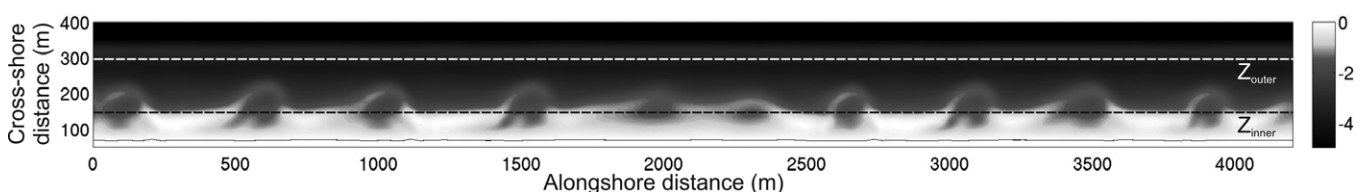


Figure 2. Evolution of the double sandbar morphology after a 12-day simulation period with constant shore-normal waves with $H_s = 0.8$ m and $T_p = 8$ s starting from the alongshore-uniform bathymetry, together with locations of $Z_{\text{inner}}(n)$ and $Z_{\text{outer}}(n)$. The key indicates elevation in m.

where dz is the uniform spacing in z_n , n is the alongshore coordinate, s is the alongshore scale (Torrence and Compo, 1998) and $*$ is the complex conjugate. In addition, we used normalized bivariate extension of the continuous wavelet transform for two discrete sequences z_n ($n = 0, \dots, N - 1$) and y_n ($n = 0, \dots, N - 1$), wavelet-squared coherency, $R_n^2(s)$ (Jevrejeva *et al.*, 2003; Grinsted *et al.*, 2004):

$$R_n^2(s) = \frac{|S\{s^{-1}W_n^{zy}(s)\}|^2}{S\{s^{-1}W_n^z(s)\}S\{s^{-1}W_n^y(s)\}}, \quad (2)$$

where S is a smoothing operator detailed in Torrence and Webster (1999) and Grinsted *et al.* (2004).

The wavelet analysis was on two alongshore lines of sea bed level (Figure 2), denoted $Z_{\text{inner}}(n)$ and $Z_{\text{outer}}(n)$ in the following. We chose the cross-shore location of $Z_{\text{inner}}(n)$ and $Z_{\text{outer}}(n)$ to be representative of the inner-bar evolution and outer-bar morphology, respectively. The $W_n^z(s)$ is used to decompose Z_{inner} and Z_{outer} into energy at a given alongshore scale and at a given alongshore distance. This enables both the detection of the dominant spatial modes of variability and how these modes vary in space. $R_n^2(s)$ is used to measure the linear relationship between $Z_{\text{inner}}(n)$ and $Z_{\text{outer}}(n)$ as a function of alongshore location and scale. A wavelet squared-coherency of 1 means a perfect linear relationship between $Z_{\text{inner}}(n)$ and $Z_{\text{outer}}(n)$ at a specific scale and alongshore distance, whereas a value of 0 is approached for vanishing linear correlation. As in a previous wavelet application to sandbar data (Ruessink *et al.*, 2007), we used the Morlet wavelet as the mother wavelet ψ_0 because of its good localization characteristics in both the space and frequency domains. Its scale is almost identical to the corresponding Fourier wavelength $\lambda = 1.03 s$ (Torrence and Compo, 1998). In all results below, the term wavelength refers to the Fourier wavelength λ equivalent to the wavelet scale s . We determined the statistical significance of $W_n^z(s)$ and $R_n^2(s)$ against synthetic red noise series, as detailed in Torrence and Compo (1998). The edge-affected part of $W_n^z(s)$ and $R_n^2(s)$ is termed the cone of influence (COI). The COI progressively reduces the useful alongshore region of analysis as the wavelength scale increases. The spatial averages (outside of the COI) of $W_n^z(s)$ and $R_n^2(s)$ are denoted $W^z(s)$ and $R^2(s)$.

3 Results

Figure 2 shows the bathymetry after a 12-day simulation starting from the alongshore-uniform geometry with $H_{s0} = 0.8$ m. The inner bar developed rip channels. The outer bar remained alongshore uniform as waves were too small with respect to the water depth above the outer-bar crest to drive sufficiently intense horizontal circulations likely to form 3D patterns. The inner-bar rip spacing is weakly alongshore variable. This alongshore variability is detailed in Figure 3 through the wavelet analysis. The alongshore non-uniform variability of the seabed along Z_{inner} has a typical amplitude on the order of one

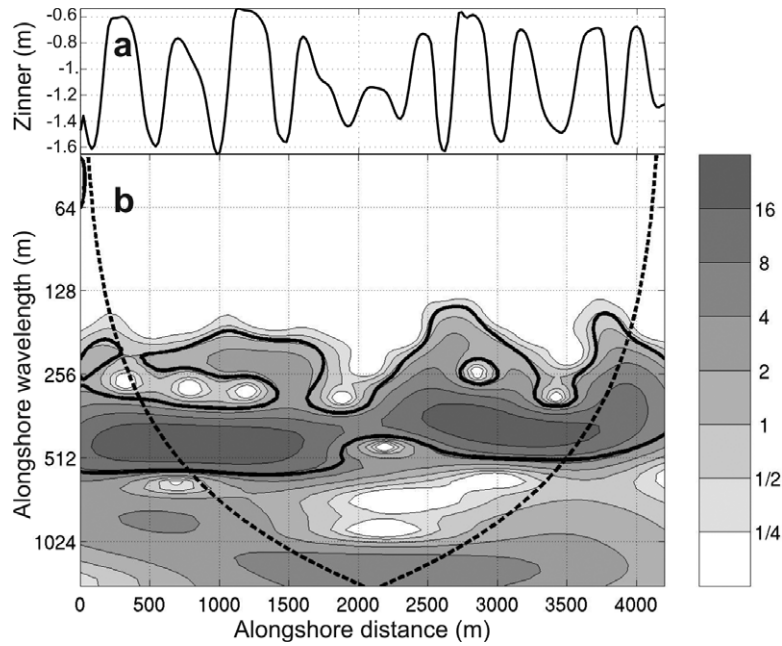


Figure 3. (a) Alongshore depth line Z_{inner} for the morphology given in Figure 2 and (b) the corresponding inner-bar local wavelet spectrum $W_n^z(s)$ normalized by the variance (shading), with the 5% significance level against red noise (bold solid contours) and the cone of influence (bold dotted curves).

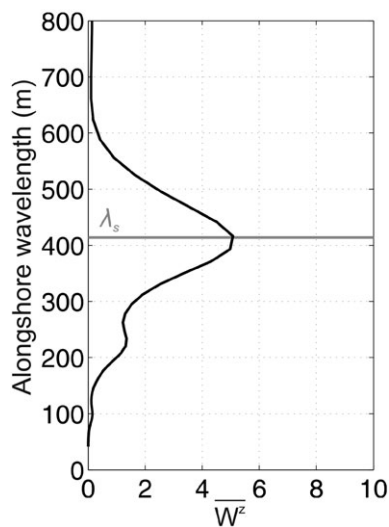


Figure 4. Alongshore-averaged wavelet spectra $\overline{W^z}(s)$ for Z_{inner} normalized with the variance in Z_{inner} , excluding local wavelet values within the COI, for the morphology given in Figure 2 and Z_{inner} in Figure 3. λ_s denotes the self-organization inner-bar emerging wavelength.

metre (Figure 3a). The local wavelet spectrum for this simulation indicates that Z_{inner} contains statistically significant power at the alongshore wavelengths λ between about 300 and 500 m, with slightly larger wavelengths at $x = 0\text{--}2000$ m than at $x = 2500\text{--}4200$ m, as is readily apparent in Figure 2. At $x = 2000\text{--}2500$ m, two less-developed inner-bar rip channels are observed. This alongshore variability in the inner-bar rip channel spacing is expected to be due to edge effects resulting from the periodic lateral boundary conditions imposed by the flow model. Given this restriction, the strong nonlinear behaviour of the inner-bar dynamics tends to self-organize into a more uniform spacing through mergings and splittings. The alongshore-averaged local wave spectrum of Z_{inner} (Figure 4) shows that the inner bar contains statistically high power at λ

$= 420$ m. This corresponds to the self-organization mechanism emerging wavelength at the inner bar and is hence denoted λ_s in Figure 4. It is to be noted that a similar λ_s is observed for $H_{s0} = 1$ m, with a similar weak alongshore variability.

In Figure 5, the bathymetries of the four situations (weakly and well-developed outer-bar crescents, both with $H_s = 0.8$ m and 1.0 m) after a few-day simulation period show remarkable differences (Figures 5b, c, e, f) in comparison with the inner-bar variability when self-organization mechanisms prevail (Figure 2). When the outer bar was initially well-developed (Figure 5a), regular features developed for $H_s = 0.8$ m with two inner-bar rip channels within one outer-bar crescent (coupling at half of the outer-bar wavelength; Figure 5b), reminiscent of the observations in Castelle *et al.* (2007). For a similar initial outer-bar geometry, with $H_s = 1$ m, regular features also developed, in this case with one rip channel facing one outer-bar horn (180° out-of-phase coupling; Figure 5c), like the patterns observed by Van Enckevort and Wijnberg (1999), Castelle *et al.* (2007) and Quartel (2009). For both $H_s = 0.8$ and 1 m, coupling mechanisms readily overwhelm self-organization mechanisms at the scale of the individual inner bar, as the inner-bar morphology is fully coupled to the outer-bar geometry. In contrast, when the outer bar was initially weakly developed (Figure 5d), highly irregular inner-bar features formed for both $H_s = 0.8$ m (Figure 5e) and $H_s = 1$ m (Figure 5f). Neither of the three regular length scales observed in the other three simulations (Figures 2, 5b and 5c) are readily apparent.

Alongshore-averaged local wave spectra and wavelet coherency-squared are shown in Figure 6 for the four final situations shown in Figure 5. When the outer crescentic bar is well-developed, $Z_{\text{inner}}(n)$ contains statistically significant high wavelet power at $\lambda = 300$ m (Figure 6a, denoted $\lambda_c/2$) and $\lambda = 600$ m (Figure 6b, denoted λ_c) for the $H_s = 0.8$ m and 1 m simulation, respectively, with λ_c the coupling wavelength (outer-bar wavelength). Both the $\lambda = 300$ m and 600 m peaks result from morphological coupling, as indicated by the high wavelet-squared coherency values for $\lambda = 600$ m in Figure 6b. Note that bivariate wavelet transforms cannot capture the coupling at 300 m by definition; this is equally true for other

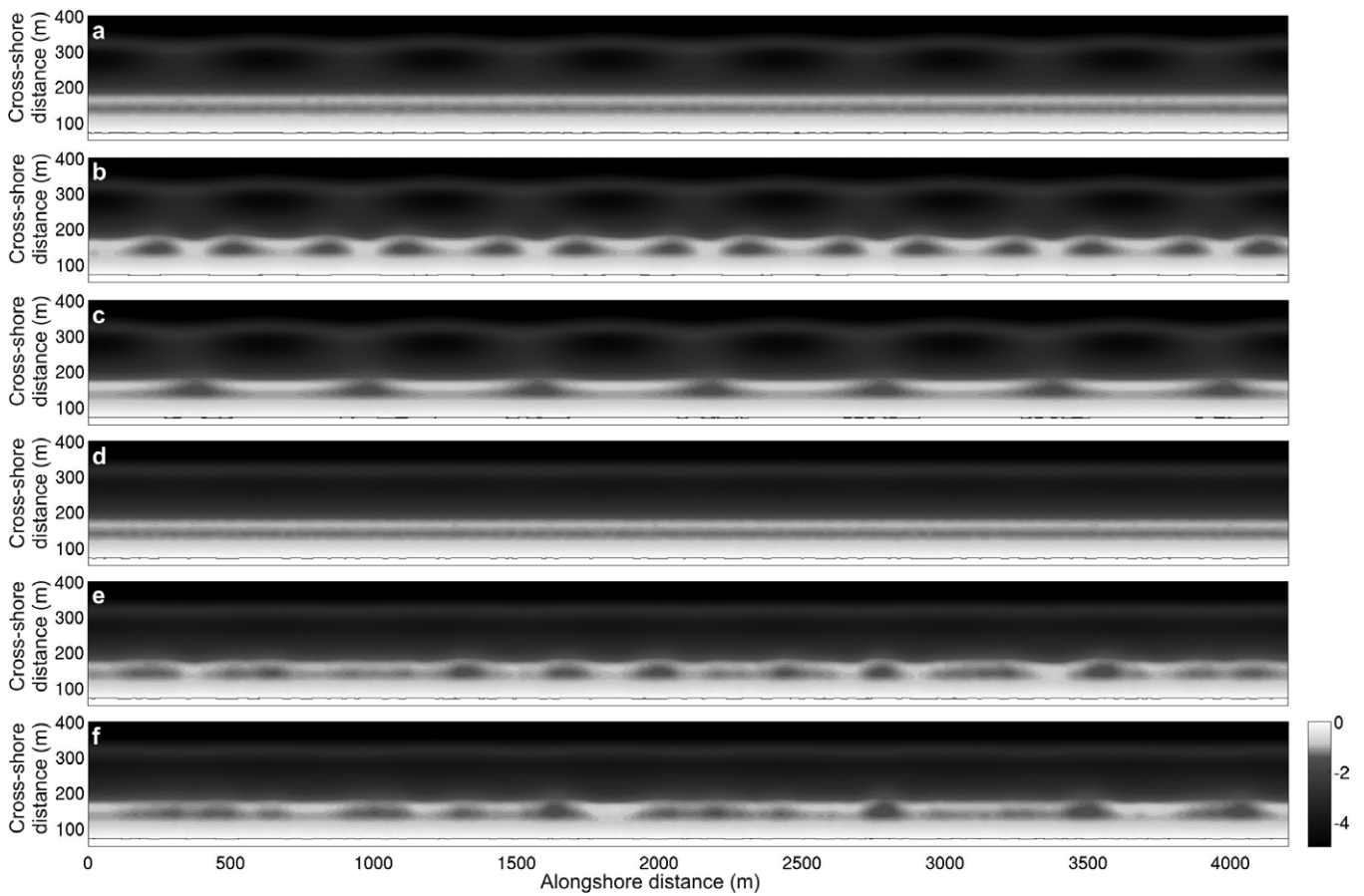


Figure 5. Evolution of the double sandbar morphology with constant shore-normal waves and $T_p = 8$ s: (a) initial well-developed outer crescentic bar, (b) evolution of (a) after a 6-day simulation period with $H_s = 0.8$ m, (c) evolution of (a) after a 4-day simulation period with $H_s = 1$ m, (d) initial weakly-developed outer crescentic bar, (e) evolution of (d) after an 8-day simulation period with $H_s = 0.8$ m, and (f) evolution of (d) after a 6-day simulation period with $H_s = 1$ m. The key indicates elevation in m.

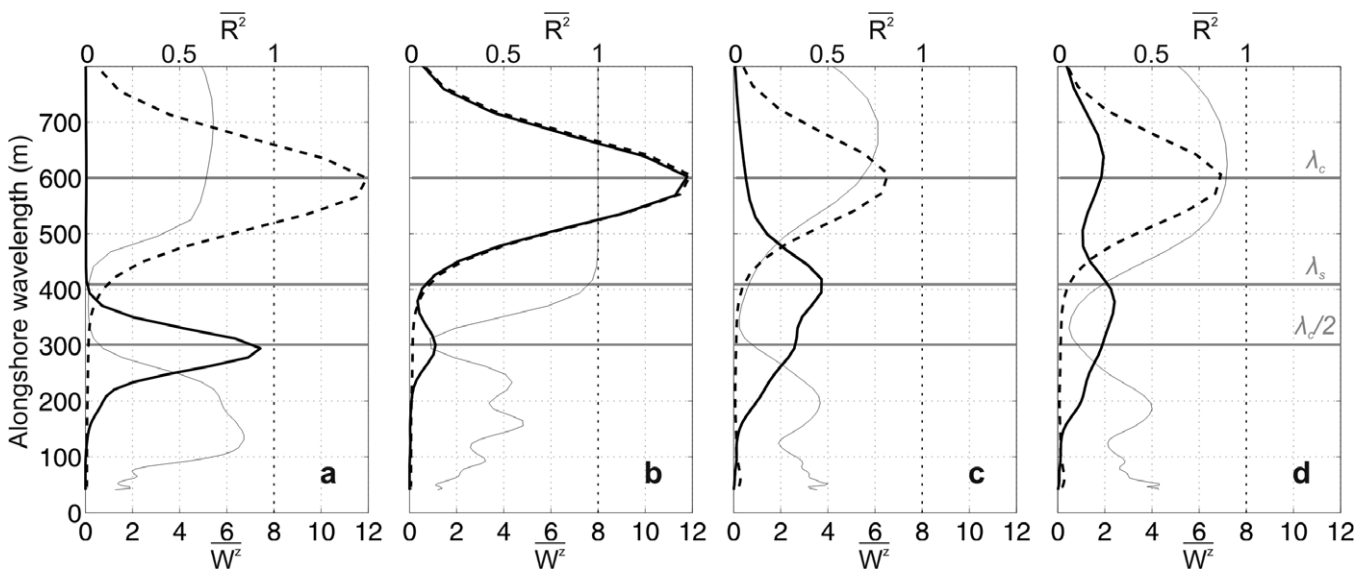


Figure 6. Alongshore-averaged wavelet spectra $\overline{W^z}(s)$ for Z_{inner} (bold solid line) and Z_{outer} (bold dashed line) and wavelet-coherency squared $R^2(s)$ between Z_{inner} and Z_{outer} (thin solid line). (a), (b), (c) and (d) correspond to the alongshore depth lines in Figures 5b, 5c, 5e and 5f, respectively. In each panel the wavelet power has been normalized with the variance in Z_{inner} and Z_{outer} respectively. We excluded local wavelet and coherency-squared values within the COI, the region of (n,s) space influenced by wavelet edge effects, in the computation of $\overline{W^z}(s)$ and $R^2(s)$. The horizontal grey lines are explained in the text.

techniques potentially suitable to detect morphological coupling, such as cross-correlation and cross-spectral analysis. For the $H_s = 0.8$ m run with weakly-developed crescentic outer-bar patterns, $Z_{inner}(n)$ contains statistically significant

power at $\lambda = 300$ m and 420 m (Figure 6c). For $\lambda = 300$ m, the statistically high power for the inner bar is indicative of coupling at half of the outer-bar wavelength, reminiscent of the coupling patterns in Figure 5b. In contrast, the $\lambda = 420$ m

is most likely due to self-organization mechanisms, as indicated by both the low $R^2(s)$ values (Figure 6c) and the wavelet results for the simulation with prevailing self-organization mechanism (Figure 4). For the $H_s = 1$ m run with weakly-developed crescentic outer-bar patterns, $Z_{\text{inner}}(n)$ contains statistically significant power at $\lambda = 600$ m and in the range of 300–420 m (Figure 6d). For $\lambda = 600$ m the $R^2(s)$ is large (Figure 6d), which, together with statistically high wavelet power for both inner and outer bars, is indicative of morphological coupling reminiscent of the 180° out-of-phase coupling observed in Figure 5c. The $\lambda = 300$ – 420 m statistically high power is most likely due to self-organization mechanisms with a significant contribution of coupling at $\lambda_c/2$ reminiscent of the weak statistical power at $\lambda_c/2$ observed in Figure 6b for the well-developed situation. It is to be noted that the 300 m and 420 m peaks are distinct during the first hours of the simulation and eventually tend to merge. For both the $H_s = 0.8$ m and $H_s = 1$ m runs, the superposition of both self-organized and morphological features results in the rather irregular inner-bar rip spacing observed in Figures 5e and 5f. The general field observation of highly alongshore-variable inner-bar rip channels contrasting with the more regular outer-bar crescents, previously thought to be a proof of no morphological coupling, is actually indicative of a mixture of self-organization and morphological coupling mechanisms. In addition, the superimposition of the two mechanisms results in smaller alongshore-averaged inner-bar rip spacing than with self-organization mechanisms alone as shown for the $H_s = 1$ m run (Figure 5f) and particularly the $H_s = 0.8$ m run (Figure 5e).

The alongshore variations of the relative importance of self-organization mechanism versus morphological coupling is assessed through the non-averaged local spectra. The non-averaged local spectra for the $H_s = 1$ m and well-developed outer-bar crescent run (Figure 7) show that inner-bar power at the coupling wavelength λ_c and local coherency-squared diagram are alongshore uniform, as expected from the regular spacing of the inner-bar rip channels in Figure 5c. A similar alongshore uniformity is observed for the $H_s = 0.8$ m and well-developed outer-bar crescent run. In contrast, the wavelet analysis for the weakly-developed outer-bar crescent run with $H_s = 1$ m ($H_s = 0.8$ m) given in Figure 8 (Figure 9) indicates that, when there is a mixture of both mechanisms, the relative importance of self-organization mechanisms versus morphological coupling is alongshore variable. For instance, in Figure 8, at alongshore distance $x = 1500$ – 4000 m, high power can be found at λ_c while high power at $\lambda_c/2 < \lambda < \lambda_s$ is restricted at $x = 1000$ – 2000 m. The alongshore variability in the relative importance of self-organization versus morphological coupling enforces the apparent highly alongshore-variable inner-bar rip channels that are observed in Figures 5e and f. Initially we suspected that the alongshore variability of the respective contributions of the two mechanisms was a lateral-boundary effect. However, when we ran an additional simulation with the alongshore domain extended to 8400 m, we found (not shown) the relative importance of self-organization mechanism versus morphological coupling to still be strongly alongshore variable, even in the (alongshore) centre of the computational domain. At this stage we do not know why the relative importance of self-organization mechanism versus morphological coupling is alongshore variable.

We also examined the ability of the model to simulate the observed double sandbar behaviour change from non-coupled to coupled (Ruessink *et al.*, 2007). To investigate this potential change, we ran an additional simulation with an initial alongshore-uniform outer bar with its crest in 2 m water depth and $H_s = 1.6$ m. The temporal evolution of the double

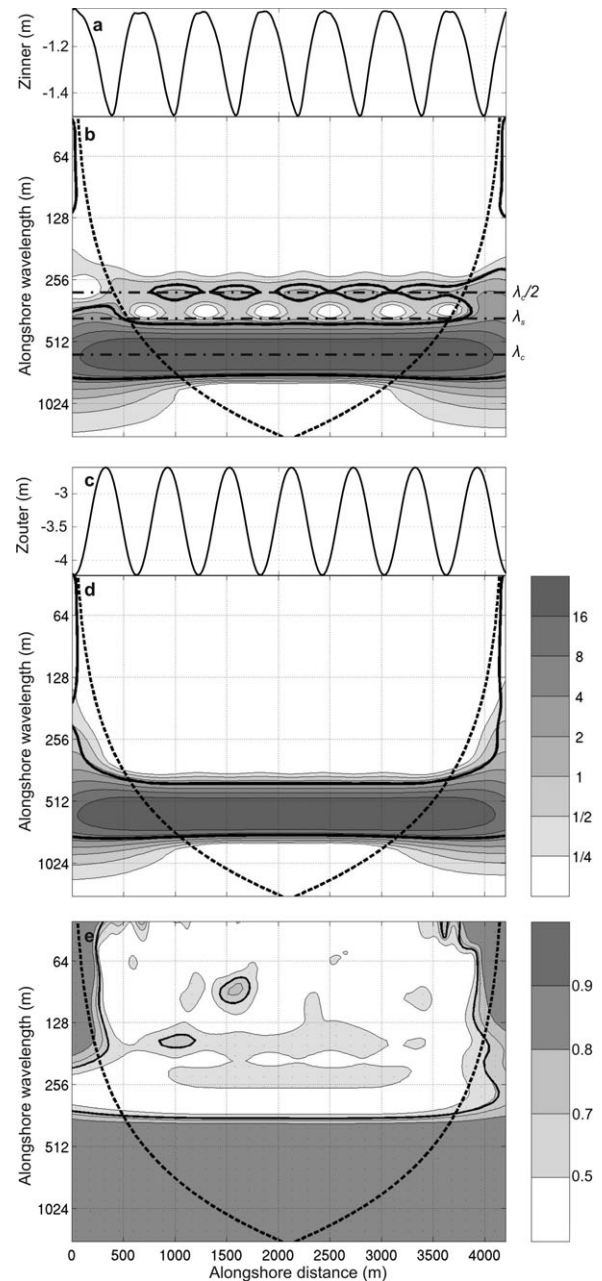


Figure 7. Wavelet analysis corresponding to Figure 5c: (a) alongshore depth line Z_{inner} (b) inner-bar local wavelet spectrum $W_n^Z(s)$, (c) alongshore depth line Z_{outer} (d) outer-bar local wavelet spectrum $W_n^Z(s)$ and (e) wavelet coherency-squared diagram $R_n^2(s)$. In each wavelet panel, the wavelet power has been normalized with the variance in Z_{inner} and Z_{outer} respectively, with the 5% significance level against red noise shown as the bold solid contours and the bold dotted curves depicting the COI beyond which edge effects become important. The horizontal black dash-dotted lines in (b) are explained in the text.

sandbar system morphology is given in Figure 10 with corresponding evolution of the non-averaged local spectra and local coherency-squared diagrams in Figure 11. Results show that after a 2-day simulation period (Figure 10a), a wide range of wavelengths is present at the beginning of inner-bar rip channel and outer-crescentic sandbar formation (Figures 11a and b). Small statistically significant coherency-squared values are observed in the whole (n,s) space, with only occasionally large statistically significant coherency-squared values for some narrow wavelength bands (for instance in Figure 11c, at $x = 3200$ – 3500 m for $\lambda \approx 120$ m) in which, however, both the

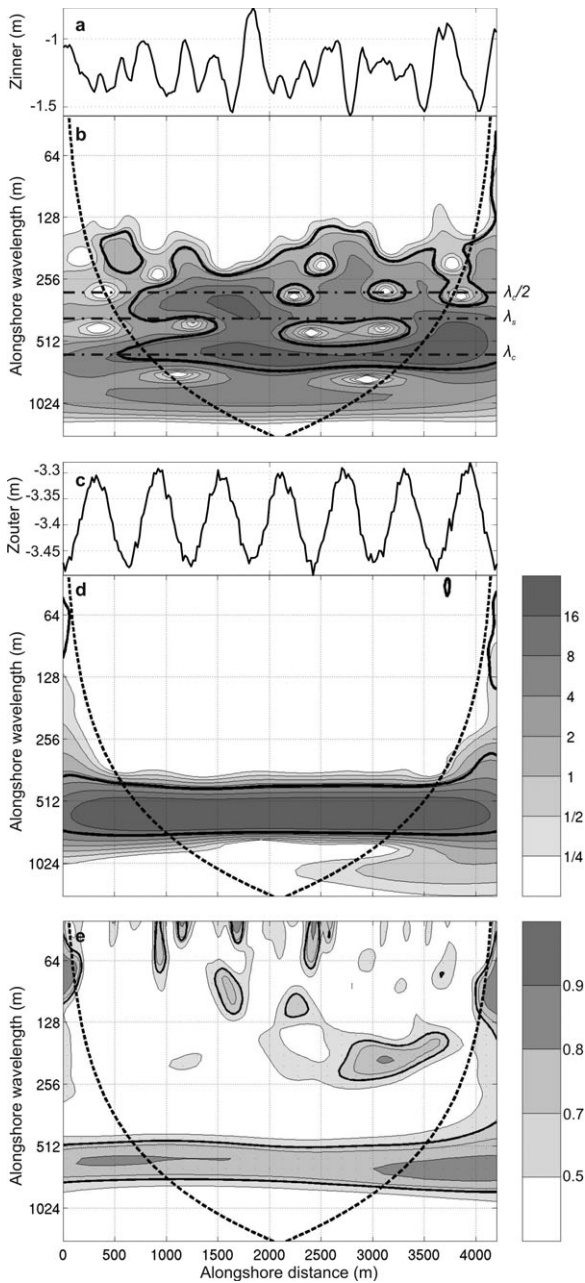


Figure 8. Wavelet analysis corresponding to Figure 5f: (a) alongshore depth line Z_{inner} , (b) inner-bar local wavelet spectrum $W_{inner}^2(s)$, (c) alongshore depth line Z_{outer} , (d) outer-bar local wavelet spectrum $W_{outer}^2(s)$ and (e) wavelet coherency-squared diagram $R_{inner}^2(s)$. In each wavelet panel, the wavelet power has been normalized with the variance in Z_{inner} and Z_{outer} respectively with the 5% significance level against red noise shown as the bold solid contours and the bold dotted curves depicting the COI beyond which edge effects become important. The horizontal black dash-dotted lines in (b) are explained in the text.

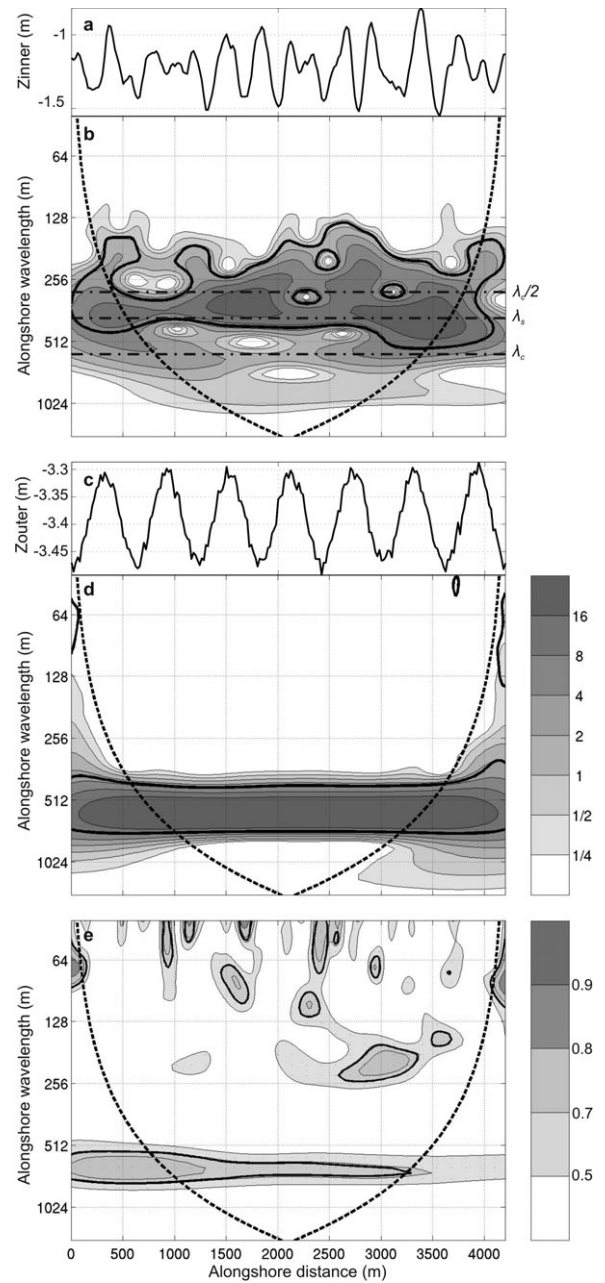


Figure 9. Wavelet analysis corresponding to Figure 5e: (a) alongshore depth line Z_{inner} , (b) inner-bar local wavelet spectrum $W_{inner}^2(s)$, (c) alongshore depth line Z_{outer} , (d) outer-bar local wavelet spectrum $W_{outer}^2(s)$ and (e) wavelet coherency-squared diagram $R_{inner}^2(s)$. In each wavelet panel, the wavelet power has been normalized with the variance in Z_{inner} and Z_{outer} respectively, with the 5% significance level against red noise shown as the bold solid contours and the bold dotted curves depicting the COI beyond which edge effects become important. The horizontal black dash-dotted lines in (b) are explained in the text.

local wavelet power for the inner and outer bar were not significant, which is indicative of non-coupling. This suggests that the development of inner bar and outer bar 3D patterns are initially spatially non-coupled. However, over time the inner-bar morphology appears to couple with that of the outer bar. After a 4-day simulation period (Figure 10b), such coupling becomes apparent at $x = 2000\text{--}3500$ m for $\lambda \approx 350$ m (Figure 11f) in which, however, the inner-bar local wavelet power is reasonably weak. After a 6-day simulation period (Figure 10c), the alongshore extent of coupling is significantly larger together with higher power for the local coherency-

squared diagram (Figure 11i) and statistically higher wavelet power in both the inner-bar (Figure 11g) and outer-bar (Figure 11h) local wavelet spectra. After an 8-day simulation period, the band with large coherency-squared values increased to lower wavelengths (Figure 11i), also encompassing regions with high inner-bar (Figure 11j) and outer-bar (Figure 11k) local wavelet power. Furthermore, statistically significant linear coupling can now be found all along the computational domain (Figure 11i). This results in the striking coupling patterns observed in Figure 10d with inner-bar rip channels systematically facing outer-bar horns (180° out-of-phase

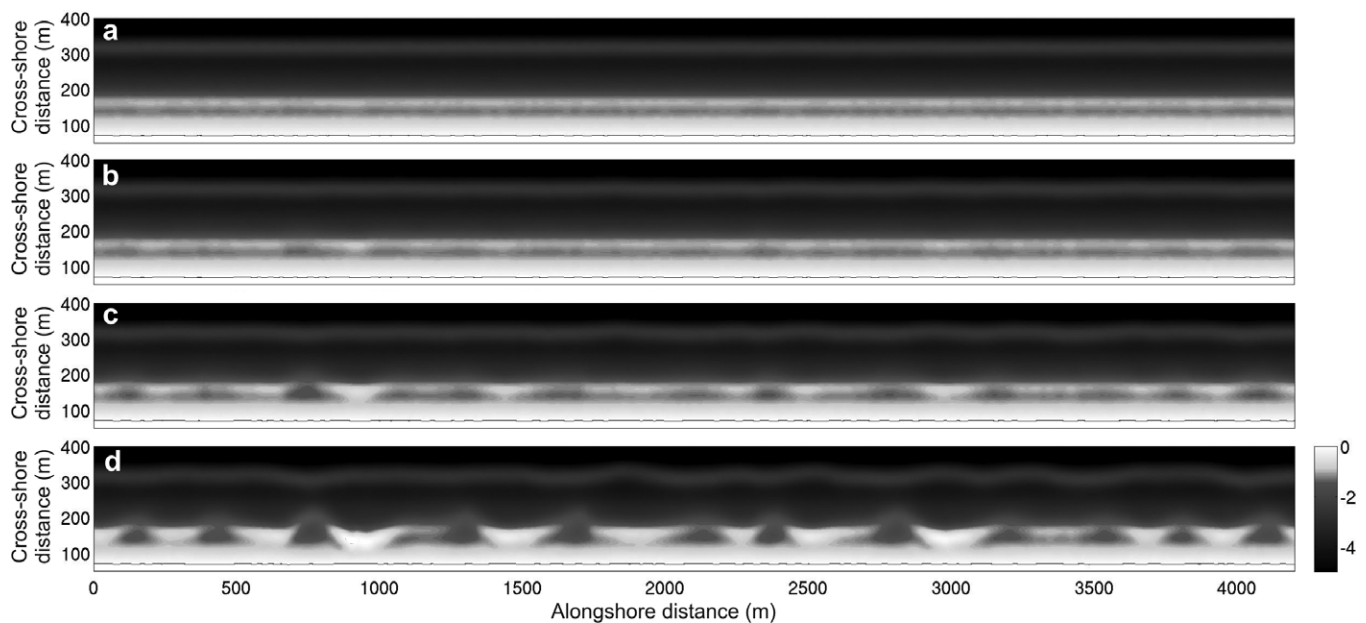


Figure 10. Evolution of the double sandbar morphology for constant shore-normal waves with $H_s = 1.6$ m and $T_p = 8$ s showing the temporal development of alongshore variability in the inner and outer bars from non-coupled to coupled. (a) $t = 2$ days, (b) $t = 4$ days, (c) $t = 6$ days, (d) $t = 8$ days. At the end of the simulation, the inner-bar rip channels systematically face the outer-bar horn (180° out-of-phase coupling).

coupling). The alongshore wavelength of the inner and outer bars are reasonably alongshore non-uniform.

4 Discussion and Conclusions

With our numerical simulations we have established that the relative importance of self-organization mechanisms and morphological coupling to the generation of inner-bar morphological variability is governed by the magnitude of the depth variations along the outer-bar crest. When the outer bar is alongshore uniform, self-organization mechanisms are predominant and the inner bar develops a rhythmicity arising from this mechanism of instability alone. This rhythmicity is found to be reasonably alongshore uniform. The small alongshore variations in the inner-bar wavelength are supposed to be due to the combination of edge effects resulting from the periodic lateral boundary conditions of the depth-averaged flow model and the strong nonlinear behaviour of the inner-bar dynamics, which tend to self-organize into a more uniform spacing through mergings and splittings (the equilibrium state is not reached). In contrast, when the outer-bar crescents are well-developed, self-organization mechanisms are overwhelmed by coupling mechanisms. In this case, inner-bar rip channels arise from horizontal circulation patterns driven by alongshore variations in wave set-up enforced by wave refraction and wave breaking across the outer bar. The relative importance of wave focusing by refraction versus wave breaking across the outer bar controls the inner-bar patterns morphologically forced by the outer bar (Part 1).

For the weakly-developed crescents, both mechanisms co-exist as shown by the wavelet analysis, resulting in highly alongshore-variable inner-bar rip channel spacing. Although such irregular variability is generally considered as proof of no morphological coupling, our work demonstrates that this variability actually arises from a mixture of self-organization and morphological coupling mechanisms. The superimposition of the two mechanisms also results in smaller spatially averaged inner-bar rip spacing than when self-organization mechanism or morphological coupling prevails. The general

field observation that inner-bar rip channels are more irregularly spaced and with smaller alongshore scales than outer-bar crescents suggests that morphological coupling may be more important to understanding and predicting the evolution of inner-bar rip channels than previously envisaged. In addition, the fact that the relative importance of each mechanism is strongly alongshore variable enforces the highly irregular alongshore variability in the inner bar.

Our model also successfully simulated the main characteristics of the coupled-noncoupled nature of double sandbar systems observed by Ruessink *et al.* (2007) under continued low-energy wave conditions following a morphological reset event (alongshore-uniform double sandbar system). A wide range of wavelengths is observed at the beginning of the 3D pattern development (for both the inner bar and outer bar), with alongshore non-uniformity development at the scale of the individual bar. A temporal change from non-coupled to coupled behaviour occurs in response to the increasingly three-dimensional outer bar. At the end of the simulation, statistically significant linear coupling can now be found along the entire computational area with inner-bar rip channels systematically facing outer-bar horns (180° out-of-phase coupling). These numerical results are essentially similar to the observations of Ruessink *et al.* (2007), despite the fact that they are highly idealized with time-invariant offshore wave conditions and mean water level. We note that, without the presence of the inner bar and with the same wave forcing, the outer bar develops reasonably similar alongshore scales as in Figure 10, confirming that in the double-bar case the inner bar couples to the outer bar, and not the other way around.

This change from non-coupled to coupled behaviour, together with the realistic coupling patterns simulated in Part 1 starting from idealized double sandbar geometry, enforce the confidence we can have in the numerical model. The nonlinear morphodynamic models used in the nearshore community (Damgaard *et al.*, 2002; Reniers *et al.*, 2004; Klein and Schuttelaars, 2006; Castelle *et al.*, 2006; Drønen and Deigaard, 2007; Smit *et al.*, 2008; Garnier *et al.*, 2008) contain the essential physics to examine the initial growth and subsequent nonlinear evolution of 3D surfzone sandbars. Limitations of

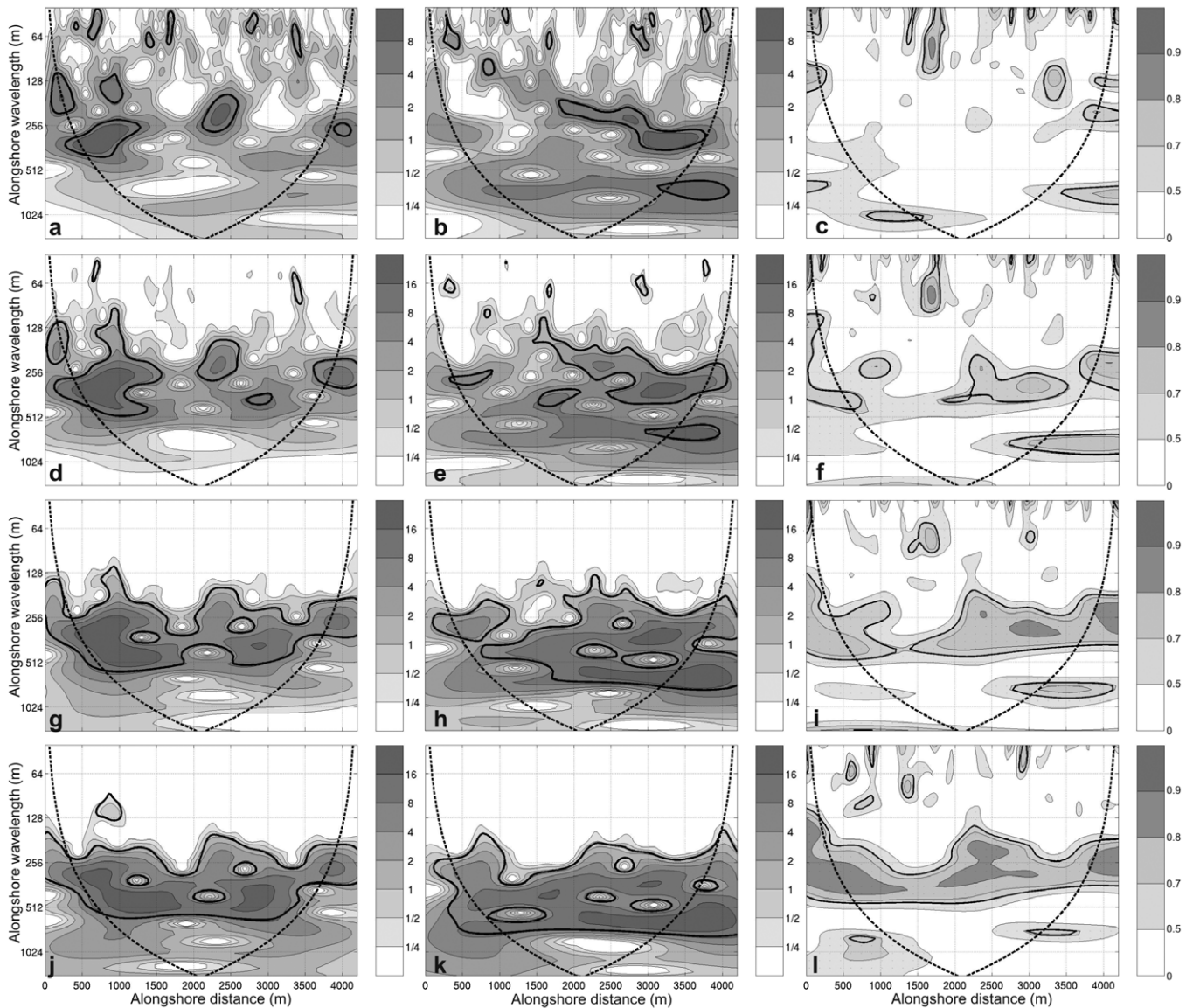


Figure 11. Wavelet analysis corresponding to Figure 10: (a, d, g, j) show the inner-bar local wavelet spectra $W_n^z(s)$, (b, e, h, k) the outer-bar local wavelet spectra $W_o^z(s)$ and (c, f, i, l) the wavelet coherency-squared diagrams $R_n^z(s)$. In each panel, the wavelet power has been normalized with the variance in Z_{inner} and Z_{outer} respectively, with the 5% significance level against red noise shown as the bold solid contours and the bold dotted curves depicting the COI beyond which edge effects become important. (a, b, c) correspond to Figure 10a, (d, e, f) to Figure 10b, (g, h, i) to Figure 10c and (j, k, l) to Figure 10d.

the modelling study undertaken in this paper for the assessment of the relative importance of self-organization mechanisms versus morphological coupling must be pointed out. The contribution of self-organization mechanisms is strongly dependent on the initial random perturbation height initially superimposed on the double sandbar geometry. For instance, for a given offshore wave height H_s and a given vertical amplitude of the horn/bay sequence D_v , decreasing the initial perturbation height favours a change from a mixture of both mechanisms to morphological coupling mechanisms overwhelming self-organization mechanisms. However, the initial random perturbation height does not have any physical sense. Therefore, the simulations and study outcomes presented in this paper constitute a proof of concept rather than a comprehensive extensive modelling exercise. The model will have to be confronted with further field data starting from an accurately surveyed bathymetry and comprising time-varying offshore wave conditions and tidal elevation.

All the simulations were run with time-invariant mean water level (no tide). However, the role of continuously changing

tidal elevation in the field may be significant to the development of inner-bar rip channels. A slight variation in mean water level results in a change of the balance between wave breaking and refraction across the outer bar. This induces a change in the driven inshore horizontal circulation patterns which are crucial to the development of inner-bar rip channels. Emergence of coupling patterns in meso- to macro-tidal environments is potentially more complicated than in the idealized simulations presented in both this paper and the companion paper, despite the fact that they were observed in such tidal settings (Ruessink *et al.*, 2007; Castelle *et al.*, 2007; Quartel, 2009). Even more importantly, tide-induced continuously changing balance between breaking and refraction across the 3D outer bar can be hypothesized to enforce the inner-bar rip channel alongshore variability. Further simulations with tides are required to examine the effects of tidal range on the alongshore variability of inner-bar rip-channel scale and how it mixes with self-organization and coupling mechanisms.

Our simulations showed that coupling mechanisms are important for understanding and predicting the evolution of

inner-bar rip channels, and the whole system, during down-state transitions (post-storm periods). Conversely, the potential role of coupling during up-state transitions is poorly documented. For instance, Wijnberg and Holman (2007) observed at a single-barred beach (Duck, USA) that, during storm events, a crescentic bar may shed a bar-like feature that later transits the trough and merges with the subaerial beach within a few days. The authors named this spatially isolated feature a Shoreward Propagating Accretionary Wave (SPAW). Almar *et al.* (in press) observed a similar SPAW event on the double-barred meso- to macro-tidal Truc Vert Beach, southwest France, during a 10-year return storm. They showed that the SPAW connected to the inner bar and subsequently influenced the inner-bar dynamics. The mechanism leading to both the formation and migration of the SPAW and its subsequent interaction with the inner-bar dynamics is not understood. In general, the role of coupling mechanisms during down-state sequence has been highlighted here and in the companion paper, but understanding and reproducing the interaction between the inner and outer bars during up-state sequence remains a challenge for future numerical studies.

Acknowledgements—The wavelet computations in this paper were based on software developed by Aslak Grinsted and co-workers (version wtc-r14, available from <http://www.pol.ac.uk/home/research/waveletcoherence/>). BC and PB gratefully acknowledge funding from the project MODLIT (under the Program RELIEFS/INSU – SHOM/DGA). BGR and TDP acknowledge financial support through the Netherlands Organisation for Scientific Research award 864.04.007 and contract 818.01.009, respectively. The authors wish to thank the two anonymous reviewers for their positive criticism that improved the quality of the paper.

References

- Aarninkhof SGJ, Hinton C, Wijnberg KM. 1998. On the predictability of nearshore bar behaviour. In *Proceedings of 26th Internat. Conference on Coastal Eng.* ASCE: New York. 2409–2422.
- Almar R, Castelle B, Ruessink BG, Sénéchal N, Bonneton P, Marieu V. in press. Two- and three-dimensional double-sandbar system behaviour under intense wave forcing and a meso-macro tidal range. *Continental Shelf Research*.
- Bailard JA. 1981. An energetics total load sediment transport model for a plane beach. *Journal of Geophysical Research* **86**: C11, 10938–10954.
- Barusseau J-P, Radulescu M, Descamps C, Akouango E, Gerbe A. 1994. Morphosedimentary multiyear changes on a barred coast (Gulf of Lions, Mediterranean Sea, France). *Marine Geology* **122**: 47–62.
- Booij N, Ris RC, Holthuijsen LH. 1999. A third-generation wave model for coastal regions, Part 1: Model description and validation. *Journal of Geophysical Research* **104**: C4, 7649–7666.
- Bowen AJ, Inman DL. 1971. Edge waves and crescentic bars. *Journal of Geophysical Research* **76**: 8662–8671.
- Bowman D, Goldsmith V. 1983. Bar morphology of dissipative beaches: an empirical model. *Marine Geology* **51**: 15–33.
- Calvete D, Dodd N, Falqués A, Van Leeuwen SM. 2005. Morphological development of rip channel systems: Normal and near-normal wave incidence. *Journal of Geophysical Research* **110**: C10006, DOI: 10.1029/2004JC002803.
- Castelle B, Bonneton P, Butel R. 2006. Modeling of crescentic pattern development of nearshore bars: Aquitanian Coast, France. *C. R. Geoscience* **338**: 795–801.
- Castelle B, Bonneton P, Dupuis H, Sénéchal N. 2007. Double bar beach dynamics on the high-energy meso-macrotidal French Aquitanian Coast: A review. *Marine Geology* **245**: 141–159.
- Castelle B, Ruessink BG, Bonneton P, Marieu V, Bruneau N, Price TD. 2010. Coupling mechanisms in double sandbar systems. Part 1: Patterns and physical explanation. *Earth Surface Processes and Landforms*, DOI: 10.1002/esp.1929.
- Coco G, Murray AB. 2007. Patterns in the sand: from forcing templates to self-organization. *Geomorphology* **91**: 271–290.
- Damgaard J, Dodd N, Hall L, Chesher T. 2002. Morphodynamic modeling of rip channel growth. *Coastal Engineering* **43**: 199–221.
- Deigaard R, Drønen N, Fredsøe J, Jensen JH, Jørgensen MP. 1999. A morphological stability analysis for a long straight barred coast. *Coastal Engineering* **36**: 171–195.
- Drønen N, Deigaard R. 2007. Quasi-three-dimensional modelling of the morphology of longshore bars. *Coastal Engineering* **54**: 197–215.
- Falqués A, Coco G, Huntley DA. 2000. A mechanism for the generation of wave-driven rhythmic patterns in the surf zone. *Journal of Geophysical Research* **105**: 24071–24088.
- Garnier R, Calvete D, Falqués A, Dodd N. 2008. Modelling the formation and the long-term behavior of rip channel systems from the deformation of a longshore bar. *Journal of Geophysical Research* **113**: C07053, DOI: 10.1029/2007JC004632.
- Goldsmith V, Bowman D, Kiley K. 1982. Sequential stage development of crescentic bars: HaHoterim Beach, Southeastern Mediterranean. *Journal of Sedimentary Petrology* **52**: 233–249.
- Greenwood B, Davidson-Arnott RGD. 1979. Sedimentation and equilibrium in wave-formed bars: A review and case study. *Canadian Journal of Earth Sciences* **16**: 312–332.
- Grinsted A, Moore JC, Jevrejeva S. 2004. Application of the cross wavelet transform and wavelet coherence to geophysical time series. *Nonlinear Processes in Geophysics* **11**: 561–566.
- Holman RA, Bowen AJ. 1982. Bars, bumps and holes: Models for the generation of complex beach topography. *Journal of Geophysical Research* **87**: 457–468.
- Hom-ma M, Sonu C. 1962. Rhythmic pattern of longshore bars related to sediment characteristics. In *Proceedings of 8th Internat. Conference on Coastal Engineering* ASCE: New York. 248–278.
- Houser C, Greenwood B. 2005. Hydrodynamics and sediment transport within the inner surf zone of a lacustrine multiple-barred nearshore. *Marine Geology* **218**: 37–63.
- Jevrejeva S, Moore JC, Grinsted A. 2003. Influence of the Arctic Oscillation and El Niño–Southern Oscillation (ENSO) on ice conditions in the Baltic Sea: The wavelet approach. *Journal of Geophysical Research* **108**: D21, DOI: 10.1029/2003JD003417.
- Klein MD, Schuttelaars HM. 2006. Morphodynamic evolution of double-barred beaches. *Journal of Geophysical Research* **111**: C06017, DOI: 10.1029/2005JC003155.
- Lafon V, De Melo Apoluceno D, Dupuis H, Michel D, Howa H, Froidefond J-M. 2004. Morphodynamics of nearshore rhythmic sandbars in a mixed-energy environment (SW France): I. Mapping beach changes using visible satellite imagery. *Estuarine, Coastal and Shelf Science* **61**: 289–299.
- Lafon V, Dupuis H, Butel R, Castelle B, Michel D, Howa H, De Melo Apoluceno D. 2005. Morphodynamics of nearshore rhythmic sandbars in a mixed-energy environment (SW France): II. Physical forcing analysis. *Estuarine, Coastal and Shelf Science* **65**: 449–462.
- Lippmann TC, Holman RA. 1990. The spatial and temporal variability of sand bar. *Journal of Geophysical Research* **95**: (C7), 11575–11590.
- Lippmann TC, Holman RA, Hathaway KK. 1993. Episodic, nonstationary behaviour of a double bar system at Duck, North Carolina, USA, 1986–1991. *Journal of Coastal Research Special issue* **15**: 49–75.
- MacMahan JH, Thornton EB, Stanton TP, Reniers AJHM. 2005. RIPEX-observations of a rip current system. *Marine Geology* **218**: 113–134.
- Masselink G. 2004. Formation and evolution of multiple intertidal bars on macrotidal beaches: Application of a morphodynamic model. *Coastal Engineering* **51**: 713–730.
- Quartel S. 2009. Temporal and spatial behaviour of rip channels in a multiple-barred coastal system. *Earth Surface Processes and Landforms* **34**: 163–176.
- Reniers AJHM, Roelvink JA, Thornton EB. 2004. Morphodynamic modeling of an embayed beach under wave group forcing. *Journal of Geophysical Research* **109**: C01030, DOI: 10.1029/2002JC001586.

- Ruessink BG, Terwindt JHJ. 2000. The behaviour of nearshore bars on the time scale of years: A conceptual model. *Marine Geology* **163**: 289–302.
- Ruessink BG, Wijnberg KM, Holman RA, Kuriyama K, Van Enkevort IMJ. 2003. Intersite comparison of interannual nearshore bar behavior. *Journal of Geophysical Research* **108**: C8, DOI: 10.1029/2002JC001505.
- Ruessink BG, Coco G, Ranasinghe R, Turner IL. 2007. Coupled and noncoupled behavior of three-dimensional morphological patterns in a double sandbar system. *Journal of Geophysical Research* **112**: C07002, DOI: 10.1029/2006JC003799.
- Short AD. 1991. Macr-meso tidal beach morphodynamics – An overview. *Journal of Coastal Research* **7**: 2, 414–436.
- Short AD, Hesp PA. 1982. Wave, beach and dune interactions in southeastern Australia. *Marine Geology* **48**: 259–284.
- Smit MWJ, Reniers AJHM, Ruessink BG, Roelvink JA. 2008. The morphological response of a nearshore double sandbar system to constant wave forcing. *Coastal Engineering* **55**: 761–770.
- Thornton EB, MacMahan JH, Sallenger AH Jr. 2007. Rip currents, mega-cusps, and eroding dunes. *Marine Geology* **240**: 151–167.
- Torrence C, Compo GP. 1998. A practical guide to wavelet analysis. *Bulletin of the American Meteorological Society* **79**: 61–78.
- Torrence C, Webster PJ. 1999. Interdecadal changes in the ENSO–Monsoon system. *Journal of Climate* **12**: 2679–2690.
- Van Enkevort IMJ, Wijnberg KM. 1999. Intra-annual changes in bar plan shape in a triple bar system. In *Proceedings of Coastal Sediments '99* 2548–2558.
- Van Enkevort IMJ, Ruessink BG, Coco G, Susuki K, Turner IL, Plant NG, Holman RA. 2004. Observations of nearshore crescentic sandbars. *Journal of Geophysical Research* **109**: C06028, DOI: 10.1029/2003JC002214.
- Wijnberg KM, Holman RA. 2007. Video-observation of shoreward propagating accretionary waves. In *Proceedings of River, Coastal and Estuarine Morphodynamics '07*. ASCE: New York. 737–743.
- Wright LD, Short AD. 1984. Morphodynamic variability of surf zones and beaches: A synthesis. *Marine Geology* **56**: 93–118.